Enhanced Velocity Diffusion along Electron-Cyclotron-Resonance Heating Characteristics Observed in Hot-Electron Energy Spectra in the Plasma Loss Cone

T. Saito, I. Katanuma, Y. Kiwamoto, T. Kariya, and S. Miyoshi
Plasma Research Center, University of Tsukuba, Sakuramura, Niiharigun, Ibaraki 305, Japan
(Received 29 June 1987)

A silicon surface-barrier detector was used to measure energy spectra of hot electrons coming out of an end cell of the GAMMA 10 tandem mirror. A hump was observed in an energy spectrum and it was attributed to enhanced velocity diffusion along heating characteristics of the third-harmonic resonance of the incident waves. Hot electrons were produced by second-harmonic electron-cyclotron-resonance heating and scattered into the loss cone. Good agreement was obtained among the observation, Fokker-Planck simulation, and the prediction from the relativistic resonance condition.

PACS numbers: 52.50.Gj, 52.55.Jd, 52.70.Nc

An important physical issue of electron-cyclotron-resonance heating (ECRH) in a mirror field has been the diffusion of electrons in velocity space.[1-6] In a tandem mirror, ECRH is supposed to create a population of hot electrons for a thermal barrier and to heat electrons at the potential peak for the raising of an ion-confining potential.[7] Velocity diffusion of electrons is a main point of the research on ECRH in tandem mirrors also. It includes Coulomb collisions and acceleration of electrons by wave fields. This acceleration appears as velocity diffusion along heating characteristics[8] and causes axial losses of electrons. These losses are not only relevant to the efficiency of hot-electron production in a tandem mirror, but they also provide an insight into mirror ECRH physics because they reflect the mechanism of velocity diffusion. There have been theoretical studies as well as basic experiments on axial losses.[8-10] In tandem mirrors, hot-electron production by second-harmonic ($2\omega_{ce}$) ECRH has been studied in several papers.[11-13] However, these papers have not discussed velocity diffusion from the viewpoint of electron losses. This paper discusses velocity diffusion of electrons on the basis of direct analyses of the energy distribution of loss electrons and presents the first experimental indication of diffusion of electrons along heating characteristics of the third-harmonic ($3\omega_{ce}$) resonance. Since the energy spectrum of the end-loss electrons is determined by the energy distribution at the loss-cone boundary, the diffusion of electrons emerges as a hump in an energy spectrum of loss electrons. We have employed a silicon surface-barrier (SSB) detector for particle analyses of loss-cone electrons ($10\ \text{keV} \leq E \leq 500\ \text{keV}$).[3,14]

The heating configuration in which microwave power is injected as a beam to avoid cavity field heating adds a new aspect to ECRH physics in a tandem mirror.[11,13] The relativistic electron-cyclotron-resonance condition at the nth harmonic is given by

$$\omega - k_{\parallel} p_{\parallel}/m - n\omega_{ce}/\gamma = 0 \ , \qquad (1)$$

where $p_{\parallel}$ is the parallel momentum of an electron, $p_{\perp}$ is the perpendicular momentum, ω_{ce} is the electron cyclotron frequency with the rest mass m_0, γ is the relativistic factor, and m ($=\gamma m_0$) is the relativistic electron mass. The incident wave has a frequency ω and a parallel wave number $k_{\parallel}$ with a finite width $\Delta k_{\parallel}$, and is spatially localized within a limited area in a mirror cell. For given $k_{\parallel}$ and ω_{ce} only electrons on curves in the momentum space given by Eq. (1) can resonate with the wave field. We call these curves heating characteristics. In the heating configuration referred to above, heating characteristics associated with each harmonic resonance are bounded in limited domains in the momentum space.[8]

Figure 1 plots contours of the strength of diffusion coefficients in the momentum space referred to the midplane of the end mirror cell for a configuration of hot-electron production in GAMMA 10. They are calculated from the quasilinear heating model[1] and are bounce averaged. These diffusion coefficients are used in our

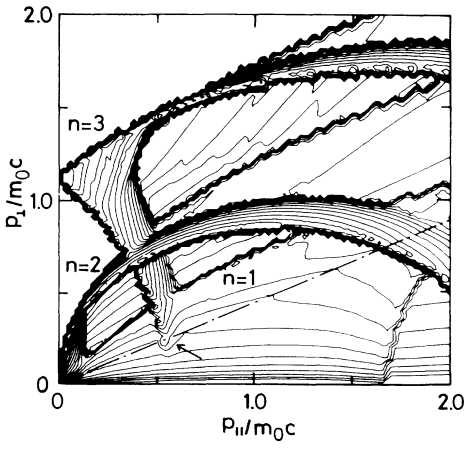

FIG. 1. Contour plot of diffusion coefficients in the momentum space for $2\omega_{ce}$ ECRH. Domains of high diffusion coefficients associated with ω_{ce}, $2\omega_{ce}$, and $3\omega_{ce}$ resonances are labeled by $n=1$, $n=2$, and $n=3$. The loss-cone boundary is shown by a dash-dotted line. The chain of the $3\omega_{ce}$ resonance crosses the loss-cone boundary as shown by the arrow.

Fokker-Planck code.[15] The calculation includes quasilinear diffusion coefficients associated with the ω_{ce}, the $2\omega_{ce}$, and the $3\omega_{ce}$ resonances. Hot electrons are produced by $2\omega_{ce}$ ECRH in an end mirror.[13] Here, $2\omega_{ce}$ ECRH means that ω is twice as high as ω_{ce} at the midplane. Microwave power of about 100 kW, with a frequency of 28 GHz, is injected as a beam aiming at the mirror midplane at an angle of 50° to the magnetic axis. The parallel refractive index $n_{\parallel}$ is 0.64. The magnetic field B_0 at the midplane is 0.497 T for the standard operation. Dark areas in Fig. 1 indicate high diffusion coefficients. There are nested domains of strong diffusion associated with the ω_{ce}, the $2\omega_{ce}$, and the $3\omega_{ce}$ resonances. We see a chain of enhanced diffusion at the $3\omega_{ce}$ resonance reaching the loss cone at an electron energy of about 100 keV (indicated by an arrow), which likely affects energy spectra of loss electrons. The $3\omega_{ce}$ resonance takes place as a result of the Doppler shift and the increase of the electron mass due to the relativistic effect. The ω_{ce} resonance stems from cavity fields existing at the 1-T region.

The SSB detector is located on an end wall of the vacuum vessel, where the magnetic field strength B is about $\frac{1}{60}$ times as high as B_0. An aluminum plate with a pinhole is placed in front of the detector to avoid a pileup of signals and the detector is surrounded by an x-ray shield. The detector is run in a pulse-height-analysis mode with an energy resolution of 10 keV. The equivalent radial position of the SSB detector mapped back to the mirror midplane along the magnetic field line (detector line) passing through the detector is about 8 cm off the axis. It detects electrons which are scattered into the loss cone on the detector line. Since the microwave beam is obliquely injected and the value of B varies along the axis, the beam crosses the detector line at $B=B_b$ ($\neq B_0$). In the present experiment B_b/B_0 is equal to 1.05.

A part of a plasma sustained by ion-cyclotron range of frequency heating in the central cell flows into the end cell. A heating pulse of $2\omega_{ce}$ ECRH is applied to the plasma target. End-loss signals detected on the SSB detector are shown in Fig. 2, together with a diamagnetic signal and a waveform of the line density at the midplane of the end cell. The diamagnetic signal increases, indicating production of hot electrons, and a train of pulses from the SSB detector appears. The pulse counting rate increases with the increasing diamagnetic signal and suddenly decreases after the turning off of the ECRH pulse. Since the diamagnetic signal decays very slowly and the density in the end cell also goes down slowly, the rate of Coulomb collisions does not change suddenly. Therefore losses of hot electrons during the $2\omega_{ce}$ ECRH pulse are induced by the electric fields of the incident microwave radiation. An energy spectrum is constructed from accumulated data of several shots with enough statistical accuracy. An energy spectrum of loss

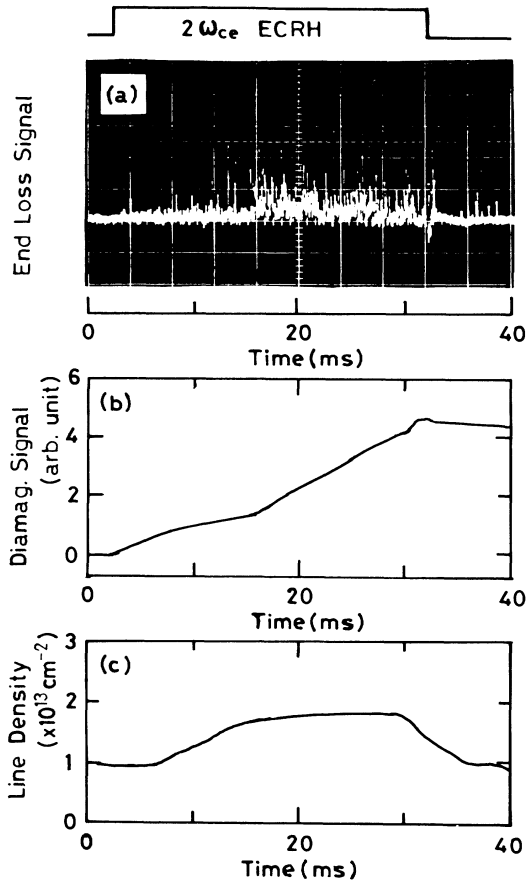

FIG. 2. Time variation of hot-electron signals obtained from a plasma shot with the standard B_0 of 0.497 T. (a) Signals of end-loss hot electrons detected on the SSB detector. The detector is artificially piled up slightly in this shot to display the signal traces clearly. (b) Diamagnetic signal in the end cell. (c) Waveform of the line density. $2\omega_{ce}$ ECRH is turned on at 2 ms and turned off at 32 ms.

electrons measured during the period from 3 to 5 ms after the turning on of $2\omega_{ce}$ ECRH is shown in Fig. 3(a). The average energy E_m estimated from the slope of the spectrum is about 20 keV. Hot electrons with high energy ($E > 100$ keV) are only slightly detected at this time. That is consistent with the measurement of electron temperature by means of x-ray analyses.[13] Electrons with higher energies are more abundantly detected later in the ECRH pulse.

In Fig. 3(b) is shown an energy spectrum measured at a later time. Electrons with energies up to 350 keV are detected and a peak appears in the energy spectrum. The most probable cause of such a peak in the energy spectrum is the scattering of electrons into the loss cone due to the $3\omega_{ce}$ resonance (see Fig. 1). The energy E_{peak} at the observed peak is nearly equal to the energy $E_{3\omega}$ of an electron which has a pitch angle θ close to the

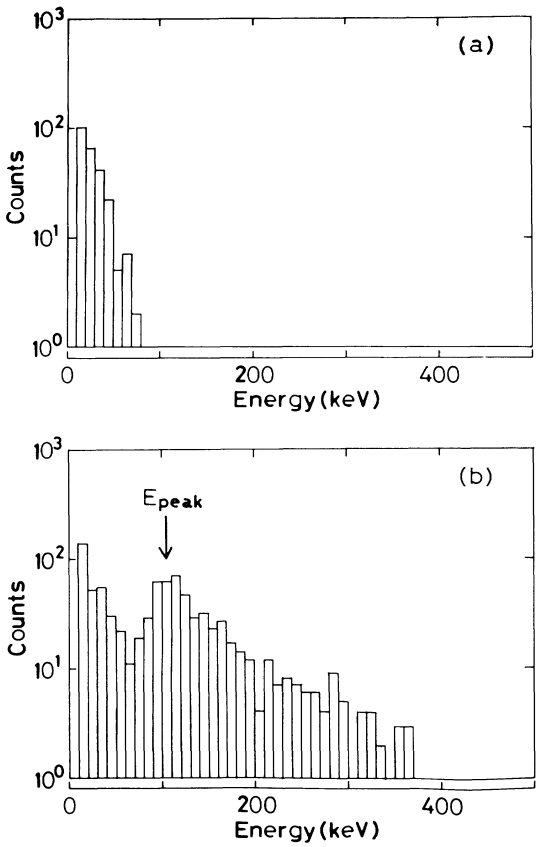

FIG. 3. Energy spectra of end-loss hot electrons obtained from analyses of SSB signals. (a) Energy spectrum obtained during the period from 3 to 5 ms after the turning on of $2\omega_{ce}$ ECRH. (b) Energy spectrum obtained at a later time.

loss-cone angle θ_{LC} and resonates with the incident electric field at the $3\omega_{ce}$ resonance. We have measured energy spectra of loss electrons for several values of B_0. A peak is clearly observed in the energy spectrum for each B_0 except for $B_0=0.33$ T. Figure 4 plots the observed E_{peak} (open circles) as a function of B_0. The value of E_{peak} decreases with decreasing B_0 to become nearly zero at 0.33 T.

The energy $E_{3\omega}$ for the $n=3$ resonance at the loss cone is obtained from Eq. (1). If we fix the pitch angle of electrons at θ_{LC}, we can calculate $E_{3\omega}=m_0c^2(\gamma-1)$ by solving Eq. (1) with $n=3$, and we plot it as a solid line in Fig. 4. In the calculation, $\omega/2\pi$ is 28 GHz, $n_\parallel$ is 0.64, and ω_{ce} is 1.05 times as high as that for B_0. The measured E_{peak} agrees with the calculated $E_{3\omega}$ within experimental error except for lower B_0. Both values become zero at 0.33 T, which is because ω is nearly 3 times ω_{ce} for $B_0=0.33$ T. Computer runs of the Fokker-Planck code are also carried out to obtain energy spectra. They also show peaks, at E_{FP}, as expected from the contour mapping of diffusion coefficients. These peaks

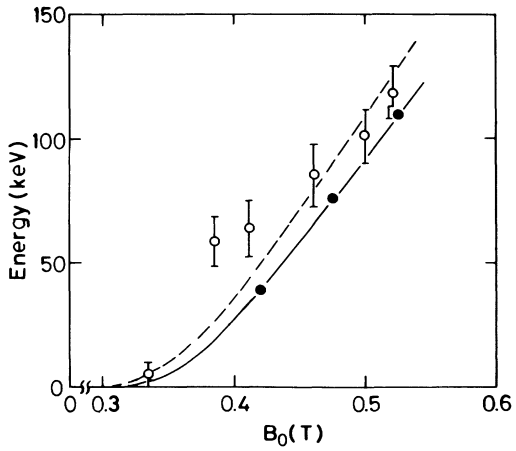

FIG. 4. Plots of energies E_{peak} (open circles), E_{FP} (filled circles), and $E_{3\omega}$ (lines) as functions of B_0. The solid line represents $E_{3\omega}$ for $B_b/B_0=1.05$ and the dashed line, for $B_b/B_0=1.08$.

are plotted in Fig. 4 as filled circles. All of E_{peak}, $E_{3\omega}$, and E_{FP} lie close to each other except for B_0 lower than 0.4 T. This indicated that the observed peaks in energy spectra stem from the scattering of electrons into the loss cone along heating characteristics of the $3\omega_{ce}$ resonance. The $3\omega_{ce}$ resonance interaction becomes very weak as the electron energy decreases. Since the incident beam of $2\omega_{ce}$ ECRH has a finite width,[13] rays within the beam of the incident wave have different $n_\parallel$ and cross the detector line at different B_b. The ray with $n_\parallel$ of 0.60 has the maximum value of B_b/B_0 equal to 1.08. The expected $E_{3\omega}$ corresponding to this ray is also plotted (by a dashed line) in Fig. 4. The dashed line lies above the solid line for $B_b/B_0=1.05$ and shows better agreement with the observations.

Loss electrons have energy spectra continuously spreading to high energy. The maximum energy of loss electrons increases in time but saturates around 400–500 keV. A small fraction of hot electrons with θ close to θ_{LC} can be heated by the $2\omega_{ce}$ resonance to that energy level. Continuous energy spectra of loss electrons do not stem directly from the $2\omega_{ce}$ resonance diffusion driven by beam fields because the associated heating characteristics connect confined electrons to the loss cone only at low energies ($E\leq 10$–20 keV) or at very high energies. However, heating characteristics associated with cavity fields can link confined electrons to the loss cone.[8] The calculation of diffusion coefficients shown in Fig. 1 includes cavity fields with the level as observed in GAMMA 10 ($\frac{1}{50}-\frac{1}{100}$ of the beam component). Diffusion coefficients of a finite magnitude are distributed in the region between the $n=2$ domain and the loss cone. This is a probable process which causes a continuous spectrum of loss electrons.

Cavity fields also cause the ω_{ce} resonance, but those

effects are estimated to be weak because of their low power level. However, when an ω_{ce} ECRH pulse aiming at the 1.0-T surface is applied, its influence on electron loss can be very strong.[10] The level of $2\omega_{ce}$ ECRH power has been kept nearly constant in the present experiment. Loss rates depend on $2\omega_{ce}$ ECRH power. The effect of ω_{ce} ECRH as well as the dependence on $2\omega_{ce}$ ECRH power will be described elsewhere.

In summary, axial loss fluxes of hot electrons have been successfully analyzed by use of a SSB detector. Enhanced loss of hot electrons induced by the electric field of $2\omega_{ce}$ ECRH was observed. In the energy spectra of loss electrons, we have found a direct indication of the diffusion of electrons along heating characteristics of the third-harmonic resonance in the velocity space.

We would like to thank members of the GAMMA 10 group for their collaboration in the course of this experiment. Computation was performed with the VP-200 computer at the Computer Center of the Institute of Plasma Physics at Nagoya University.

[1]C. F. Kennel and F. Engelmann, Phys. Fluids **9**, 2377 (1966).

[2]H. Grawe, Plasma Phys. **11**, 151 (1969); J. C. Sprott and R. H. Edmonds, Phys. Fluids **14**, 2703 (1971); M. A. Lieberman and A. J. Lichtenberg, Plasma Phys. **15**, 125 (1973).

[3]H. Ikegami *et al.*, Nucl. Fusion **13**, 351 (1973).

[4]I. B. Bernstein and D. C. Baxter, Phys. Fluids **24**, 108 (1981).

[5]T. D. Rognlien, Nucl. Fusion **23**, 163 (1983).

[6]A. J. Lichtenberg *et al.*, Phys. Fluids **29**, 1061 (1986).

[7]B. W. Stallard, IEEE Trans. Plasma Sci. **12**, 134 (1984).

[8]T. D. Rognlien, Phys. Fluids **26**, 1545 (1983).

[9]A. J. Lichtenberg and G. Melin, Phys. Fluids **16**, 1660 (1973).

[10]M. E. Mauel, Phys. Fluids **27**, 2899 (1984).

[11]B. W. Stallard, Y. Matsuda, and W. M. Nevins, Nucl. Fusion **23**, 213 (1983).

[12]R. A. James *et al.*, Phys. Fluids **29**, 2748 (1986).

[13]Y. Kiwamoto *et al.*, Phys. Fluids **29**, 2781 (1986).

[14]M. J. Berger *et al.*, Nucl. Instrum. Methods **69**, 181 (1969).

[15]I. Katanuma *et al.*, Phys. Fluids **30**, 1142 (1987).